Cyclic AMP is sufficient for triggering the exocytic recruitment of aquaporin-2 in renal epithelial cells

Dorothea Lorenz[1], Andrey Krylov[1], Daniel Hahm[1], Volker Hagen[1], Walter Rosenthal[1,2+], Peter Pohl[1] & Kenan Maric[1]*

[1]Forschungsinstitut für Molekulare Pharmakologie, Berlin, Germany, and [2]Freie Universität, Berlin, Germany

The initial response of renal epithelial cells to the antidiuretic hormone arginine vasopressin (AVP) is an increase in cyclic AMP. By applying immunofluorescence, cell membrane capacitance and transepithelial water flux measurements we show that cAMP alone is sufficient to elicit the antidiuretic cellular response in primary cultured epithelial cells from renal inner medulla, namely the transport of aquaporin-2 (AQP2)-bearing vesicles to, and their subsequent fusion with, the plasma membrane (AQP2 shuttle). The AQP2 shuttle is evoked neither by AVP-independent Ca^{2+} increases nor by AVP-induced Ca^{2+} increases. However, clamping cytosolic Ca^{2+} concentrations below resting levels at 25 nM inhibited exocytosis. Exocytosis was confined to a slow monophasic response, and readily releasable vesicles were missing. Analysis of endocytic capacitance steps revealed that cAMP does not decelerate the retrieval of AQP2 from the plasma membrane. Our data suggest that cAMP initiates an early step, namely the transport of AQP2-bearing vesicles towards the plasma membrane, and do not support a regulatory function for Ca^{2+} in the AQP2 shuttle.

INTRODUCTION

In mammals, water homeostasis is regulated by epithelial cells of the renal collecting duct. Key components in the regulation of collecting-duct osmotic water permeability (P_f) are the vasopressin V_2 receptor (V_2R) and the water channel protein aquaporin-2 (AQP2). This is evident from mutations in the human V_2R and AQP2 genes causing congenital nephrogenic diabetes insipidus (Rosenthal *et al.*, 1992; Deen *et al.*, 1994). In a first step, the antidiuretic hormone arginine vasopressin (AVP) binds to V_2R expressed in principal cells, which are the main epithelial cell type of the collecting duct in the inner medulla. Stimulation of V_2R leads to an increase in cyclic AMP levels. The subsequent phosphorylation of AQP2 by cyclic AMP-dependent protein kinase (PKA) is followed by the exocytic insertion of AQP2 into the plasma membrane, resulting in an increase in P_f. This process might be accompanied by an inhibition of AQP2 endocytosis (Agre *et al.*, 2000). However, the relative contributions of exocytosis and endocytosis to P_f changes and the molecular mechanisms controlling them are not known. Two recent reports suggest that both an increase in cAMP levels and in the cytosolic Ca^{2+} concentration ($[Ca^{2+}]_i$) are required for the AQP2 shuttle and the accompanying increase in P_f (Chou *et al.*, 2000; Yip, 2002). We found that cAMP is the sole trigger of the AQP2 shuttle and that cytosolic Ca^{2+} is not able to promote or evoke the AQP2 shuttle in primary cultured inner-medulla collecting-duct cells from rat kidney (IMCD cells); in this, IMCD cells differ from other systems that display slow Ca^{2+}-independent exocytosis (Hille *et al.*, 1999).

RESULTS

Ca^{2+} transients and the AQP2 shuttle

The basal $[Ca^{2+}]_i$ level in IMCD cells was 187 ± 15 nM (number of cells $n = 45$; mean $\pm$ s.e.m.). AVP-stimulation increased $[Ca^{2+}]_i$ by 108 ± 14 nM ($n = 45$) (Fig. 1A, left panel) in 80% of the cells. Of the responding cells, 64% exhibited a time-invariant increase in $[Ca^{2+}]_i$, in 13% $[Ca^{2+}]_i$ decayed to baseline within 60 s, and in 23% $[Ca^{2+}]_i$ oscillations (frequencies 0.025–0.01 Hz) were observed. In all cells, $[Ca^{2+}]_i$ was distributed homogenously. The AVP-stimulated AQP2 shuttle is shown in Fig. 1A (right panel).

To elucidate the role of Ca^{2+} in this shuttle, $[Ca^{2+}]_i$ was clamped to 50 nM (Fig. 1B, left panel), 25 nM (Fig. 1C, left panel) and resting levels (150 nM) (Fig. 1D, left panel). Within the resolution limit of the fluorescence microscope, no subdomains with higher $[Ca^{2+}]_i$ were observed. Subsequent stimulation with AVP failed to induce the AQP2 shuttle only at a $[Ca^{2+}]_i$ of 25 nM (Fig. 1C, right panel). In all other cases, the AQP2 redistribution was fully preserved (Fig. 1B, D, right panel, and E). $[Ca^{2+}]_i \gg 1$ μM, achieved by treatment of cells with 10 μM ionomycin in the presence of 1.8 mM extracellular $CaCl_2$, neither initiated the AQP2 shuttle in the absence of AVP nor promoted the AVP-induced shuttle (data not shown).

Capacitance measurements to monitor exocytosis

Fusion of vesicles with the plasma membrane increases electrical cell membrane capacitance, C_m. C_m for unstimulated IMCD cells in the monolayer was 12.1 ± 0.6 pF ($n = 48$). C_m for isolated cells, obtained by pretreatment of the monolayer for 15–30 min with a Ca^{2+}-free and Mg^{2+}-free external solution containing 1 mM EGTA, was

[1]Forschungsinstitut für Molekulare Pharmakologie, Robert-Rössle-Strasse 10, D-13125 Berlin, Germany
[2]Institut für Pharmakologie, Freie Universität, Thielallee 67-73, D-14195 Berlin, Germany
*Present address: Bundesministerium für Gesundheit, Am Propsthof 78a, 53113 Bonn.
+Corresponding author. Tel: + 49 30 94793100; Fax. +49 30 94793109;
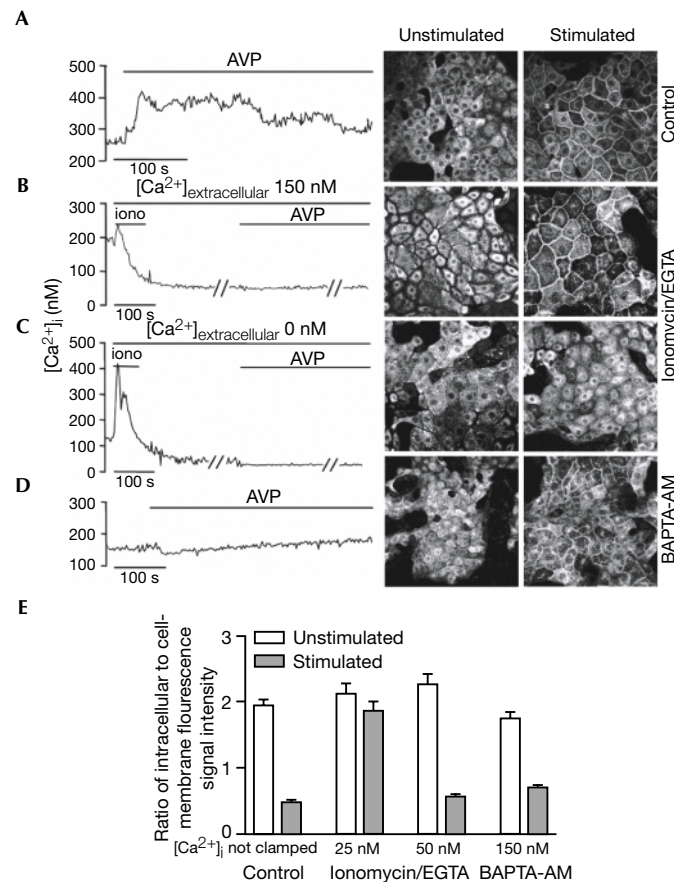E-mail: rosenthal@fmp-berlin.de

Fig. 1 | Effect of $[Ca^{2+}]_i$ in IMCD cells (left) on the AQP2 shuttle (centre and right) induced by 100 nM AVP. (**A**) AQP2 redistribution from intracellular vesicles to the plasma membrane without buffering of $[Ca^{2+}]_i$. (**B, C**) $[Ca^{2+}]_i$ was clamped by incubation of cells for 11 min in hypertonic DMEM medium containing 3.7 mM EGTA and 1.8 mM $CaCl_2$ (**B**) or 2 mM EGTA without $CaCl_2$ (**C**). During the first minute, the cells were incubated with ionomycin (iono; 10 μM) for equilibration of $[Ca^{2+}]_i$ with the extracellular medium. After an initial release of Ca^{2+} from intracellular stores, $[Ca^{2+}]_i$ reached steady state. (**D**) $[Ca^{2+}]_i$ was clamped to resting values (150 nM) by cell treatment for 30 min with 50 μM BAPTA-AM. (**E**) Ratios of intracellular to cell-membrane fluorescence (more than 1 and less than 1 indicate a predominantly intracellular and a plasma-membrane localization of AQP2, respectively).

similar (11.8 ± 0.9 pF; *n* = 17). Thus, significant electrical coupling between cells in the monolayer did not occur.

Fast application of AVP increased C_m by 1.1 ± 0.015 pF, or 9.1 ± 1.4% (*n* = 10) (Fig. 2A and C). Fusion of vesicles larger than 280 nm in diameter yielded stepwise increases in C_m (more than 2.5 fF; Fig. 2A, box). The fusion of smaller vesicles led to smooth increases in C_m, accounting for 77% of the total increase. Treatment of IMCD cells with the V_2R antagonist SR121463A (supplied by Claudine Serradeil-Le Gal (Serradeil-Le Gal *et al.*, 1996)) for 15 min before the application of AVP inhibited the response to AVP (Fig. 2A and C), indicating the involvement of V_2R. The effect of extracellularly applied AVP was mimicked by an intracellular application of cAMP through the patch pipette (Fig. 2A and C).
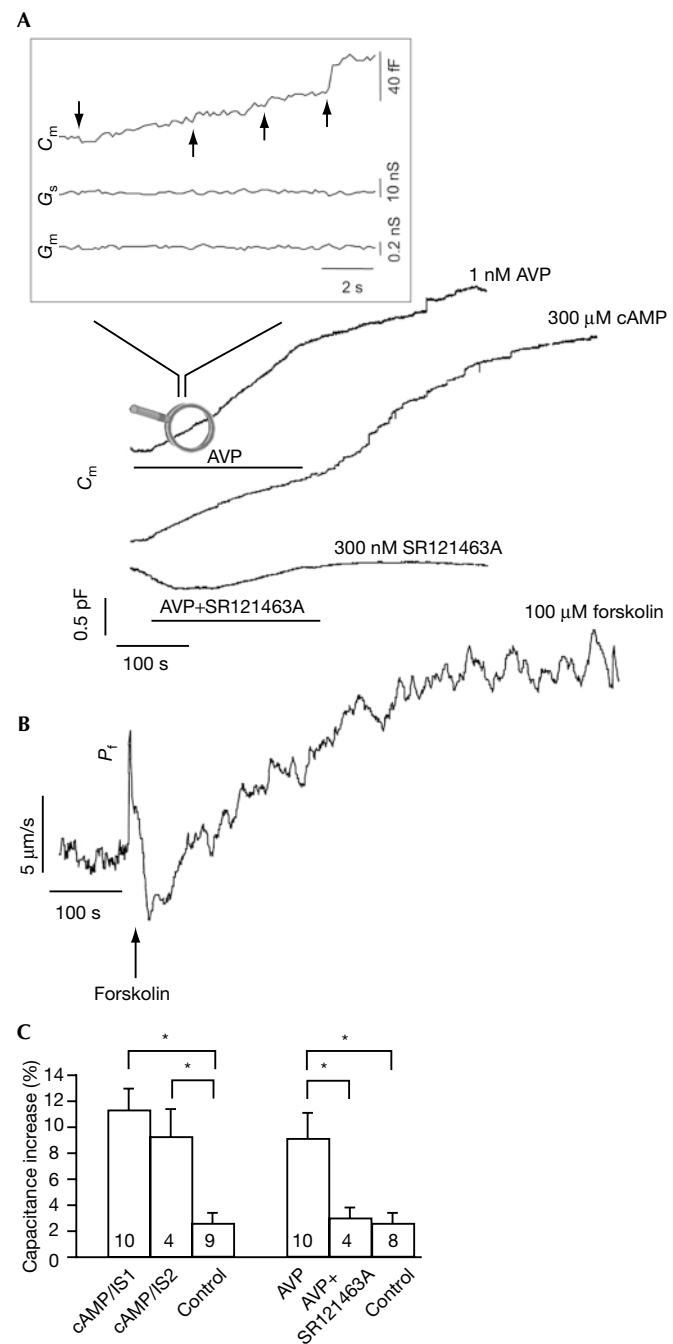

Fig. 2 | Dynamics of changes in C_m and P_f. (**A**) C_m records of IMCD cells (whole-cell configuration) exposed to 1 nM AVP, 300 μM cAMP or 1 nM AVP plus 300 nM SR121463A (V_2R antagonist). AVP and SR121463A were pressure-ejected (0.4 μl s^{-1}) from an application pipette at ~100 μm distance from the cell. cAMP was dialysed through the patch pipette. Box, expanded C_m, electrical cell membrane (G_m) and series (G_s) conductance traces (arrows indicate detectable C_m steps). (**B**) P_f time course of the IMCD cell monolayer stimulated with 100 μM forskolin. (**C**) Summarized results of increases in C_m 400 s after stimulation. Pipette solution IS1 had low Ca^{2+}-buffering capacity; pipette solution IS2 was clamped to 40 nM free Ca^{2+}. Numbers in the columns are numbers of cells; error bars show s.e.m. Asterisk indicates $P < 0.005$ (*t*-test).

When the weakly Ca^{2+}-buffering internal pipette solution (IS1) was replaced by the strongly Ca^{2+}-buffering internal solution (IS2, containing 40 nM free Ca^{2+}), the increase in C_m in response to cAMP was similar to that observed with IS1 (Fig. 2C). The data show that increases in $[Ca^{2+}]_i$ are not required for triggering exocytosis in IMCD cells.

Besides aquaporins, which (at pH 7.4) are known to exclude ions (Pohl *et al.*, 2001), cAMP upregulates epithelial Na^+ channels. However, the lack of increase in plasma membrane conductance,

$G_{m'}$ (Fig. 2A, box) suggests that neither plentiful Na^+-channel insertion into the plasma membrane nor activation of already inserted channels occurred. The result is consistent with the finding that the abundance of epithelial Na^+ channels in non-overexpressing cells is too low to determine whether cAMP alters their cell surface expression (Snyder, 2002).

Microelectrode-based P_f measurements

If the cAMP-triggered exocytosis reflects the fusion of AQP2-bearing vesicles with the plasma membrane, the time courses of increases in C_m and P_f should be identical. In agreement with this prediction, forskolin increased P_f from 13 ± 2 to 26 ± 3 µm s^{-1} with a rate similar to that of C_m (Fig. 2B). Steady-state measurements ($n = 20$; Fig. 3A) revealed the same result. Bis-(*o*-aminophenoxy)ethane-*N*,*N*,*N'*,*N'*-tetraacetic acid acetoxymethyl ester (BAPTA-AM) did not reduce the incremental P_f (Fig. 3A). Forskolin also doubled P_f in the presence of BAPTA-AM, whereas the PKA inhibitor H89, used as a control agent, abolished the stimulating effect of forskolin (Fig. 3B). These results confirm that an increase in $[Ca^{2+}]_i$ does not promote the AQP2 shuttle.

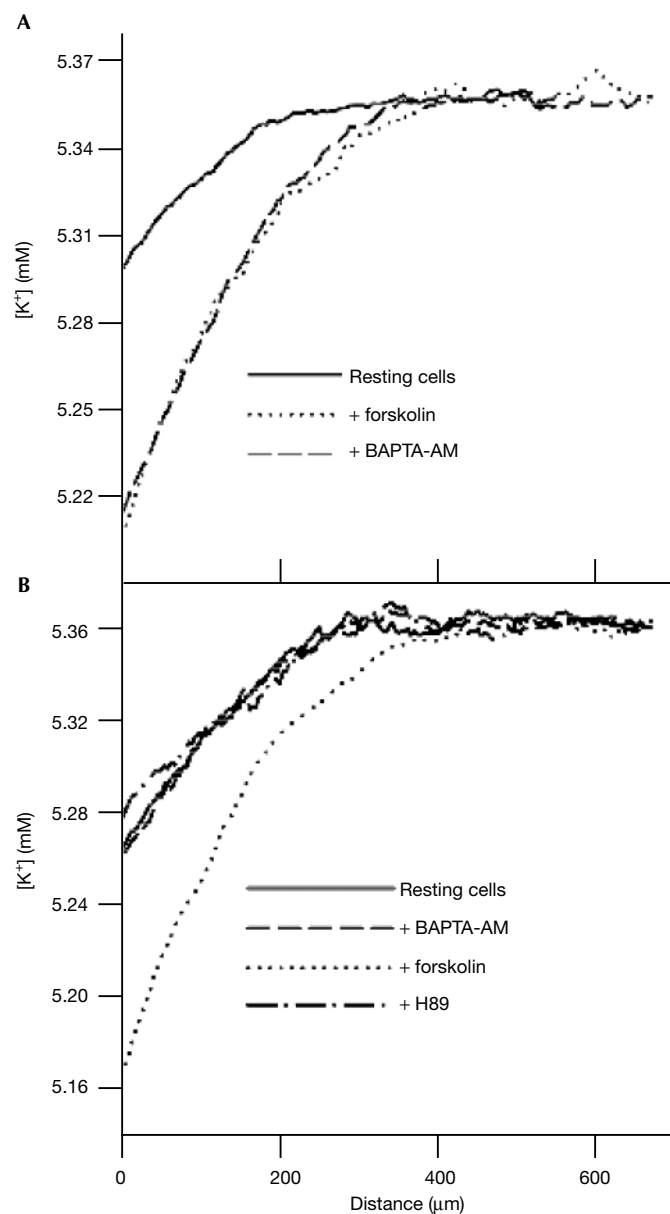**Fig. 3** | Osmotic water-flux-induced steady-state K^+ dilution allowed the calculation of P_f. (**A**) Resting cells ($P_f = 12$ µm s^{-1}) were stimulated with 50 µM forskolin (26 µm s^{-1}). Addition of 50 µM BAPTA-AM did not significantly alter water permeability. (**B**) P_f of the resting monolayer (16 µm s^{-1}) was not significantly altered by 50 µM BAPTA-AM. Subsequent stimulation with 50 µM forskolin resulted in an increase in P_f to 32 µm s^{-1}, which was reversed to 12 µm s^{-1} by 30 µM H89.
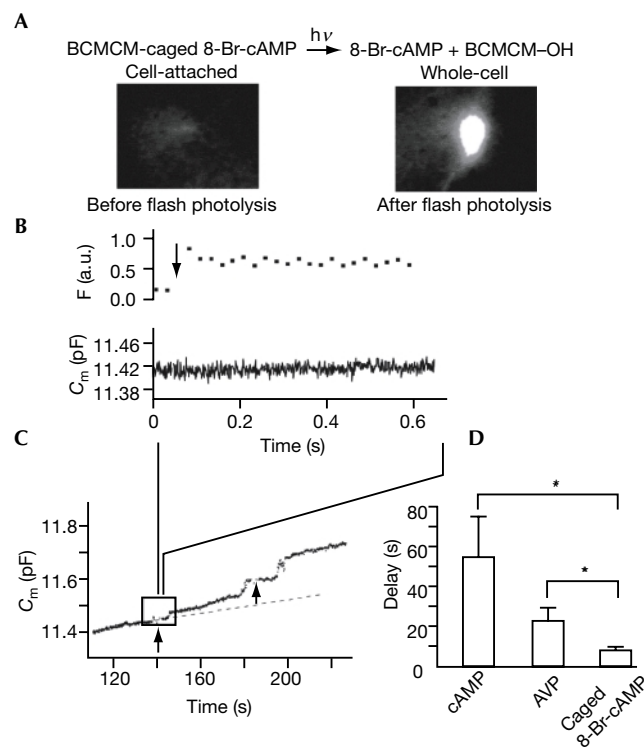

Fig. 4 | C_m recordings after flash photolysis of intracellularly applied BCMCM-caged 8-Br-cAMP (500 µM). (**A**) Visualization of the photoproduct fluorescence in living IMCD cells before (left) and after (right) flash-induced photolysis (excitation at 347 nm for 0.3 s; emission at more than 400 nm). (**B**) High-time-resolution recordings of fluorescence F (a.u., arbitrary units; 10 ms excitations) and C_m (794 Hz) before and after the first flash. (**C**) Low-time-resolution recordings from the same cell. The dotted line shows the baseline before the flash; arrows indicate flash delivery. (**D**) Time delays between stimulation and the onset of exocytosis for different stimuli; error bars show s.e.m. Asterisk indicates $P < 0.05$ (*t*-test).
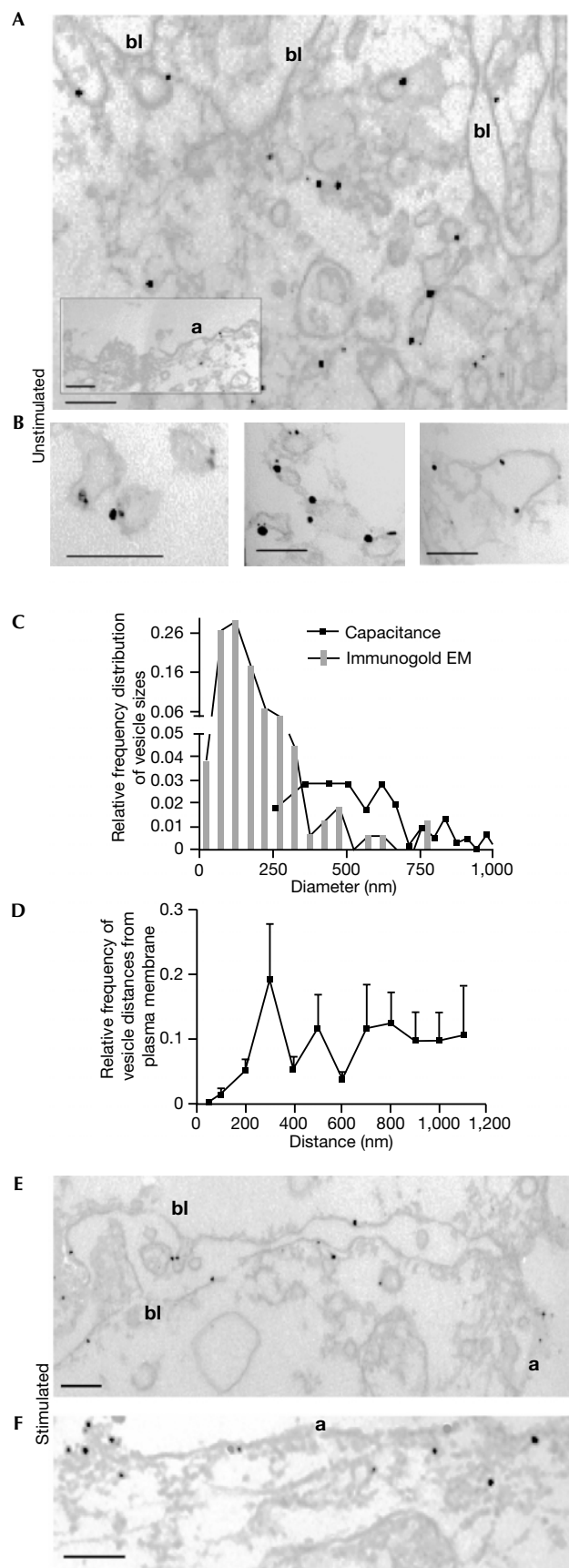
Fig. 5 | Localization of AQP2 by immunogold EM. (**A**) AQP2-bearing vesicles in resting cells. Apical (a) and basolateral (bl) plasma membranes show no gold labelling. (**B**) Single vesicles at higher magnification (scale bar, 200 nm). (**C**) Size distribution of gold-labelled vesicles compared with the vesicle sizes derived from C_m steps (more than 280 nm). (**D**) Relative frequency of AQP2-bearing vesicles as a function of the distance from the plasma membrane (eight cells). The vesicles were sorted into 100-nm bins. The first bin was subdivided into two bins of 50 nm. (**E, F**) After stimulation with forskolin (100 µM, 30 min), AQP2 is localized predominantly at the plasma membrane (a and bl). Control cells, incubated (1) without primary antibody, (2) with normal goat serum instead of primary antibody and (3) with gold-labelled BSA instead of secondary antibody revealed no staining (not shown).

Triggering of exocytosis by flash photolysis of caged cAMP

IMCD cells required 24 ± 6 s ($n = 10$) or 55 ± 19 s ($n = 10$) to respond with an increase in C_m to AVP or cAMP, respectively (Figs 2A, C and 4D). To exclude diffusion restrictions, we employed a new type of caged cAMP, the [6,7-bis(carboxymethoxy)coumarin-4-yl]methyl (BCMCM) ester of 8-Br-cAMP (BCMCM-caged 8-Br-cAMP), which, after flash photolysis, liberates within a few nanoseconds the active compound 8-Br-cAMP and a fluorescent, inactive photoproduct, 6,7-bis(carboxymethoxy)-4-(hydroxymethyl)coumarin (BCMCM-OH) (Hagen *et al.*, 2001). In the presence of strongly (IS2) and weakly (IS1) Ca^{2+}-buffering solutions in the patch pipette, increases in C_m followed the ultraviolet flash with a delay of 8 ± 2 s ($n = 10$) and 11 ± 4 s (n=4), respectively, whereas photoproduct fluorescence confirmed 8-Br-cAMP release within milliseconds (Fig. 4A, B and C). Although, significantly shortened (Fig. 4D), the persistence of the delay indicates that a pool of readily releasable vesicles is missing from IMCD cells.

AQP2 immunogold electron microscopy (EM)

In resting IMCD cells, AQP2 was found almost exclusively in vesicles (Fig. 5A, B and C). Most AQP2-bearing vesicles (99%) were found more than 50 nm away from the plasma membrane (Fig. 5D); 15% were 280–850 nm in diameter (Fig. 5C). The size distribution was in reasonable agreement with that calculated from C_m steps (Fig. 5C). After stimulation with forskolin, the gold particles decorated the apical and basolateral membranes (Fig. 5E and F).

Histogram analyses of exocytic and endocytic steps

In resting cells, exocytosis was balanced by endocytosis (Fig. 6A). Whereas the number of endocytic events remained nearly unchanged after stimulation with cAMP or AVP, the number of exocytic events clearly increased (Fig. 6B and C). Thus, at least within 10 min after application of the stimulus, IMCD cells responded with a selective increase in exocytic events.

DISCUSSION

The present study shows that the AQP2 shuttle in renal epithelial (principal) cells is exclusively triggered by cAMP. It is neither evoked nor promoted by increasing $[Ca^{2+}]_i$. However, clamping $[Ca^{2+}]_i$ at 25 nM abolished the AQP2 shuttle, indicating a requirement for Ca^{2+} at very low levels. Although there is no direct proof that only the fusion of AQP2-bearing vesicles contributes to the observed increase in C_m, the similarity of time courses of increases in P_f and C_m together with immunofluorescence and EM data strongly suggest that increases in C_m reflect exocytosis of AQP2-bearing vesicles. The delay and slow kinetics of both increases in C_m and P_f as well as the

distance of AQP2-bearing vesicles from the plasma membrane are consistent with the view that cAMP initiates the long-range targeting of AQP2 to the plasma membrane. It remains possible that—besides the distance from the plasma membrane—the lack of the release readiness of vesicles (Kasai, 1999) contributes to the slow response. The release readiness and fusion of vesicles might not be regulated by cAMP. At present we cannot exclude a role of low levels of $[Ca^{2+}]_i$ at these final steps of the AQP2 shuttle.

In contrast with our results, elimination of increases in $[Ca^{2+}]_i$ in isolated collecting ducts from rat kidney was reported to inhibit the AVP-induced AQP2 shuttle and the accompanying increase in P_f (Chou *et al.*, 2000; Yip, 2002). In collecting ducts, a $[Ca^{2+}]_i$ transient lasting 100 s seemed to be important for an increase from a resting value of 100 µm s^{-1} to 300 µm s^{-1} that was reached after 10–20 min. There is at present no explanation for the unexpectedly high resting P_f because (1) water moves primarily transcellularly (Kovbasnjuk *et al.*, 1998) and (2) the number of water channels in the apical membrane

of resting cells is rather low (Nielsen *et al.*, 1995). Thus, in the resting collecting duct, water transport is limited by the P_f of the apical epithelial membrane, which, according to measurements on bilayers reflecting its composition, is 5 µm s^{-1} (Hill & Zeidel, 2000; Krylov *et al.*, 2001). This value is in good agreement with our P_f of the resting IMCD monolayer and with the P_f of single IMCD cells obtained by laser-scanning reflection microscopy (Maric *et al.*, 2001).

The AVP-induced increase in the P_f of principal cells is due to enhanced exocytosis. Within the first 10 min, AVP does not decelerate endocytosis and hence does not prolong the persistence of AQP2 in the plasma membrane, if one assumes that decreases on C_m reflect the endocytosis of AQP2-bearing vesicles. Our data support the hypothesis that recruitment of AQP2 to the plasma membrane and its retrieval into a pool of intracellular vesicles are independently regulated events (Zelenina *et al.*, 2000).

The number of cellular systems showing a slow exocytic response while lacking a fast response is very limited. As well as principal cells, they include insulin-responding cells (adipocytes and skeletal muscle cells) and pancreatic exocrine acinar cells activated by cholecystokinin or acetylcholine. However, the signalling cascades (Yang *et al.*, 2002) leading to slow exocytic responses in these cells differ fundamentally from the cascade inducing the AQP2 shuttle in principal cells. Given the differences of regulated exocytosis in principal cells and in other cells, namely the triggering signal molecule (solely cAMP, solely Ca^{2+} or a synergistic action of both) and the kinetics (exclusively slow, exclusively fast or biphasic kinetics), the AQP2 shuttle differs from known types of exocytosis. A major challenge for future research is the identification and characterization of the cellular compartment in which cAMP initiates AQP2 targeting to the plasma membrane.
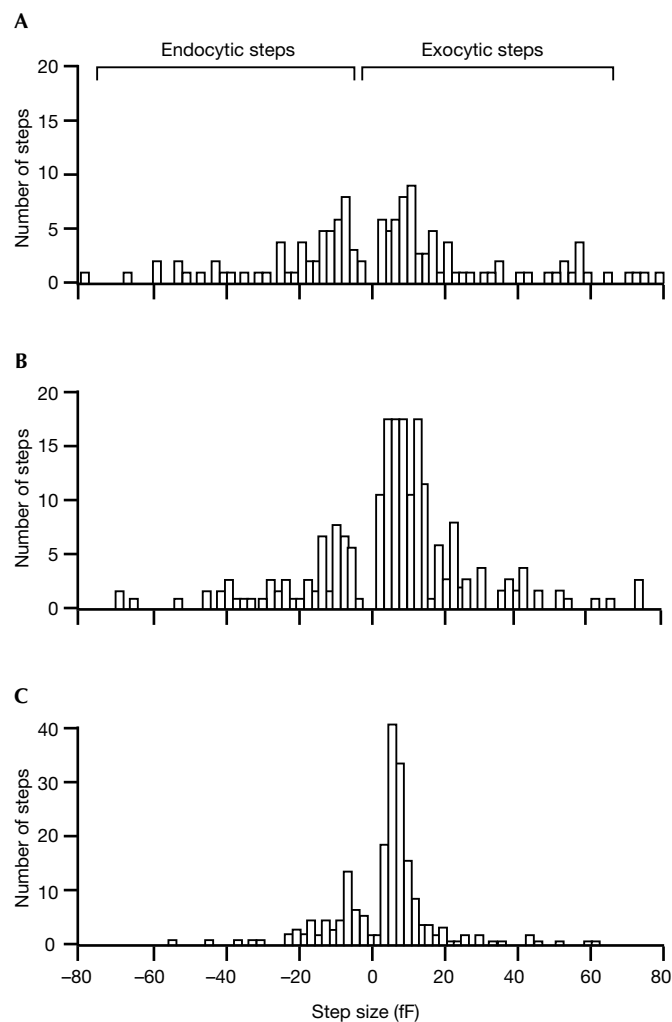
Methods

Cell culture. IMCD primary cultures (Maric *et al.*, 1998) were used from days 4 to 8 after seeding.

Ratiometric measurements of $[Ca^{2+}]_i$. IMCD cells in the monolayer were incubated (45 min) in 5 µM fura-2/AM and 0.02% Pluronic F 127 (both from Molecular Probes, Leiden, The Netherlands). Calculation of $[Ca^{2+}]_i$ (Lorenz *et al.*, 1998) was possible in 20% of the cells that showed sufficient fura-2 uptake.

Immunofluorescence. For the detection of AQP2, confocal laser-scanning microscopy was performed with a specific anti-rat AQP2 antibody and a Cy3-conjugated anti-rabbit secondary antibody (Maric *et al.*, 1998).

Cell membrane capacitance measurements. IMCD cells were transferred to the external solution (in mM: 140 NaCl, 5 KCl, 2 CaCl$_2$, 1 MgCl$_2$, 10 HEPES, 15 glucose; pH 7.2; 298 mOsm kg^{-1}) 15 min before measurement. The standard pipette solution 1 (IS1) contained (in mM) 135 potassium glutamate, 22 NaCl, 1 MgCl$_2$, 10 HEPES, 0.2 MgATP, 0.3 NaGTP, 0.2 EGTA (pH 7.2; 295 mOsm kg^{-1}). Pipette solution 2 (IS2) was similar to IS1 but was adjusted to 40 nM free Ca^{2+} with 5 mM EGTA and 1 mM CaCl$_2$.

C_m, series (G_s, 4–15 MΩ) and membrane (G_m) conductances were measured at 32–35 °C in the whole-cell configuration with an EPC-9 amplifier with the lock-in extention to Pulse software (Heka Elektronik, Lambrecht, Germany). Sinusoid stimuli (794 Hz, 60 mV peak-to-peak; 20–40 ms duration) were superimposed over the d.c. holding potential of −50 mV. Currents were sampled at 8 kHz and filtered at 1.6 kHz. The generated C_m, G_s and G_m were averaged (time resolution 8–11 Hz).

Fig. 6 | Frequency distribution of the sizes of exocytic and endocytic events (histogram bin size 2 fF). Resolvable C_m steps (more than 2.5 fF) accounting for ~23% of the increase in C_m, were analysed (Hartmann *et al.*, 1995) in unstimulated (**A**), cAMP-stimulated (**B**) and AVP-stimulated (**C**) cells. The probability that a detected step was a false positive was less than 0.002.

P_f of a confluent epithelial monolayer. Water, passing through the IMCD cell monolayer grown on a Transwell filter, diluted K$^+$ ions in the basolateral compartment that contained the osmolyte (0.4 M sorbitol). P_f was derived from microelectrode-aided measurements of (1) the steady-state K$^+$ concentration distribution adjacent to the basolateral membrane (Pohl *et al.*, 1997) and (2) the time course of K$^+$ concentration changes 20 μm away from the epithelium (see Supplementary Information).

Flash photolysis of BCMCM-caged 8-Br-cAMP. BCMCM-caged 8-Br-cAMP was synthesized by analogy with BCMCM-caged cAMP (Hagen *et al.*, 2001). Flash photolysis liberated 8-Br-cAMP and the fluorescent compound BCMCM-OH (see Supplementary Information).

Immunogold EM. IMCD cells grown on Transwell-polycarbonate filters (Costar, Bodenheim, Germany) were fixed and permeabilized (Maric *et al.*, 1998). For immunogold labelling, monolayers were incubated (16 h, 4 °C) with specific anti-rat AQP2 antibody (diluted 1:600), followed by washing and incubation (5 h, 37 °C) with secondary gold-labelled (1 nm) anti-rabbit antibody (diluted 1:200; British BioCell International, Cardiff, UK). Cells were postfixed (1% glutaraldehyde, 10 min) and treated with OsO$_4$ (2%, 1 h). After silver enhancement of gold particles (Hacker *et al.*, 1988), the samples were embedded in Epon 812, sectioned (60 nm) and stained with uranyl acetate and lead citrate before examination with a Zeiss 902 A electron microscope at 80 kV (Lorenz *et al.*, 1998).

Supplementary data are available at *EMBO reports* Online (http://www.emboreports.org).

REFERENCES

Agre, P., Nielsen, S. & Knepper, M.A. (2000) in *The Kidney. Physiology and Pathophysiology* (ed. Seldin, D.W. & Giebisch, G.) 363–377. Lippincott Williams & Wilkins, Philadelphia.

Chou, C.L. *et al.* (2000) Regulation of aquaporin-2 trafficking by vasopressin in the renal collecting duct—roles of ryanodine-sensitive Ca^{2+} stores and calmodulin. *J. Biol. Chem.*, **275**, 36839–36846.

Deen, P.M.T. *et al.* (1994) Requirement of human renal water channel aquaporin-2 for vasopressin-dependent concentration of urine. *Science*, **264**, 92–95.

Hacker, G.W. *et al.* (1988) Silver acetate autometallography: an alternative enhancement technique for immunogold-silver staining (IGSS) and silver amplification of gold, silver, mercury, and zinc in tissues. *J. Histotechnol.*, **11**, 213–221.

Hagen, V. *et al.* (2001) Highly efficient and ultrafast phototriggers for cAMP and cGMP by using long-wavelength UV/VIS-activation. *Angew. Chem. Int. Ed.*, **40**, 1045–1048.

Hartmann, J., Scepek, S. & Lindau, M. (1995) Regulation of granule size in human and horse eosinophils by number of fusion events among unit granules. *J. Physiol. (Lond.)*, **483**, 201–209.

Hill, W.G. & Zeidel, M.L. (2000) Reconstituting the barrier properties of a water-tight epithelial membrane by design of leaflet-specific liposomes. *J. Biol. Chem.*, **275**, 30176–30185.

Hille, B., Billiard, J., Babcock, D.F., Nguyen, T. & Koh, D.S. (1999) Stimulation of exocytosis without a calcium signal. *J. Physiol. (Lond.)*, **520**, 23–31.

Kasai, H. (1999) Comparative biology of Ca^{2+}-dependent exocytosis: implications of kinetic diversity for secretory function. *Trends Neurosci.*, **22**, 88–93.

Kovbasnjuk, O.N., Leader, J.P., Weinstein, A.M. & Spring, K.R. (1998) Water does not flow across the tight junctions of MDCK cell epithelium. *Proc. Natl Acad. Sci. USA*, **95**, 6526–6530.

Krylov, A.V., Pohl, P., Zeidel, M.L. & Hill, W.G. (2001) Water permeability of asymmetric planar lipid bilayers: leaflets of different composition offer independent and additive resistances to permeation. *J. Gen. Physiol.*, **118**, 333–340.

Lorenz, D. *et al.* (1998) Mechanism of peptide-induced mast cell degranulation. Translocation and patch-clamp studies. *J. Gen. Physiol.*, **112**, 577–591.

Maric, K., Oksche, A. & Rosenthal, W. (1998) Aquaporin-2 expression in primary cultured rat inner medullary collecting duct cells. *Am. J. Physiol.*, **275**, F796–F801.

Maric, K. *et al.* (2001) Cell volume kinetics of adherent epithelial cells measured by laser scanning reflection microscopy: determination of water permeability changes of renal principal cells. *Biophys. J.*, **80**, 1783–1790.

Nielsen, S. *et al.* (1995) Vasopressin increases water permeability of kidney collecting duct by inducing translocation of aquaporin-CD water channels to plasma membrane. *Proc. Natl Acad. Sci. USA*, **92**, 1013–1017.

Pohl, P., Saparov, S.M. & Antonenko, Y.N. (1997) The effect of a transmembrane osmotic flux on the ion concentration distribution in the immediate membrane vicinity measured by microelectrodes. *Biophys. J.*, **72**, 1711–1718.

Pohl, P., Saparov, S.M., Borgnia, M.J. & Agre, P. (2001) High selectivity of water channel activity measured by voltage clamp: analysis of planar lipid bilayers reconstituted with purified AqpZ. *Proc. Natl Acad. Sci. USA*, **98**, 9624–9629.

Rosenthal, W. *et al.* (1992) Molecular identification of the gene responsible for congenital nephrogenic diabetes insipidus. *Nature*, **359**, 233–235.

Serradeil-Le Gal, C. *et al.* (1996) Characterization of SR 121463A, a highly potent and selective, orally active vasopressin V$_2$ receptor antagonist. *J. Clin. Invest.*, **98**, 2729–2738.

Snyder, P.M. (2002) The epithelial Na$^+$ channel: cell surface insertion and retrieval in Na$^+$ homeostasis and hypertension. *Endocr. Rev.*, **23**, 258–275.

Yang, J., Hodel, A. & Holman, G.D. (2002) Insulin and isoproterenol have opposing roles in the maintenance of cytosol pH and optimal fusion of GLUT4 vesicles with the plasma membrane. *J. Biol. Chem.*, **277**, 6559–6566.

Yip, K.P. (2002) Coupling of vasopressin-induced intracellular Ca^{2+} mobilization and apical exocytosis in perfused rat kidney collecting duct. *J. Physiol. (Lond.)*, **538**, 891–899.

Zelenina, M. *et al.* (2000) Prostaglandin E$_2$ interaction with AVP: effects on AQP2 phosphorylation and distribution. *Am. J. Physiol. Renal Physiol.*, **278**, F388–F394.

Supplementary information

***P_f* of a confluent epithelial monolayer.** The cell monolayer grown on a Transwell-polycarbonate membrane was vertically mounted in a Teflon chamber that thereby was divided into two compartments. The hypertonic DMEM solutions in both compartments were stirred continuously to guarantee an invariant size of the unstirred layers (USL) in the immediate epithelial vicinity. The USL thickness, δ, is defined in terms of the K^+ concentration gradient at the membrane water interface:

$$\frac{|C_s - C_b|}{\delta} = \left.\frac{fC}{fx}\right|_x$$

(1)

where x is the distance from the membrane. C_b and C_s denote the K^+ concentrations in the bulk and at the interface, respectively. Osmotic water flux was induced by addition of 0.4 M D-sorbitol to the basolateral compartment. The resulting K^+ dilution in the hypertonic compartment was used to derive P_f. Therefore, K^+ concentration was measured (i) in the steady-state as a function of the distance to the surface of the epithelial cells and (ii) after stimulation with forskolin as a function of time at a distance of 20 μm away from the epithelium ($C_{20}(t)$).

Steady state P_f: C(x) measured within the USL ($-\delta < x < \delta$), can be used to derive the linear velocity of the osmotic volume flow, v (Pohl et al., 1997):

$$C(x) = C_s e^{\frac{-vx}{D} + \frac{ax^3}{3D}}$$

(2)

where D and a are the K^+ diffusion coefficient and the stirring parameter, respectively. v allows calculation of P_f:

$$P_f(t) = \frac{v}{V_W C_{osm}}$$

(3)

where V_w is the partial molar volume of water, C_{osm} the osmolyte concentration, corrected (i) for dilution by water flux and (ii) by the osmotic coefficient (here 1.09).

P_f after stimulation with forskolin: Because in a well stirred system, δ does not depend on v, C_s was expressed from a combination of the Eqs. 1 and 2. Subsequently, Eq. 2 was used to derive $v(t)$ as a function of $C_{20}(t)$, where $vx/D >> ax^3/3D$. For the hypertonic USL we got:

$$P_f(t) = \frac{D[C_{20}(t) - C_b]}{C_{osm}V_W[C_{20}(t)\delta - C_b x]}$$

(4)

The K^+ sensitive microelectrodes were made of glass capillaries, the tips (1 - 2 μm in diameter) of which where filled with cocktail B of K^+ Ionophore I (Fluka). Movement of the electrodes relative to the epithelial monolayer was realized by a hydraulic stepdrive (Narishige, Japan) with a velocity of 3 – 5 μm/s.

Flash photolysis of BCMCM-caged 8-Br-cAMP. The [6,7-bis(carboxymethoxy)coumarin-4-yl]methyl (BCMCM) ester of 8-Br-cAMP (BCMCM-caged 8-Br-cAMP) was synthesized in analogy to BCMCM-caged cAMP (Hagen et al., 2001). Flash photolysis of

BCMCM-caged 8-Br-cAMP was induced by a Xenon flash-lamp (Till Photonics, Martinsried, Germany) coupled to a Zeiss Axiovert TV135 microscope (Fluar 40x, 1.3, oil immersion objective, Carl Zeiss, Jena, Germany). The release of 8-Br-cAMP was observed by monitoring the fluorescence emitted from the liberated photoproduct 6,7-bis(carboxymethoxy)-4-(hydroxymethyl)coumarin (BCMCM-OH), using excitation at 347 nm (polychromatic illumination system, Till Photonics). The fluorescence immediately before and after the flash (10 ms excitations) was collected through a dichroic mirror FT 395, a 400 nm long pass filter (both Carl Zeiss), detected by a photodiode and acquired simultaneously with C_m, G_m and G_s data by the EPC-9. Fluorescence images of the cells were captured as described (Lorenz et al., 1998).

REFERENCES

Hagen,V., J.Bendig, S.Frings, T.Eckardt, S.Helm, D.Reuter, and U.B.Kaupp. (2001) Highly efficient and ultrafast phototriggers for cAMP and cGMP by using long-wavelength UV/VIS-activation. *Angew. Chem. Int. Ed.*, **40,** 1045-1048.

Lorenz,D., B.Wiesner, J.Zipper, A.Winkler, E.Krause, M.Beyermann, M.Lindau, and M.Bienert. (1998) Mechanism of peptide-induced mast cell degranulation. Translocation and patch-clamp studies. *J. Gen. Physiol.*, **112,** 577-591.

Pohl,P., S.M.Saparov, and Y.N.Antonenko. (1997) The effect of a transmembrane osmotic flux on the ion concentration distribution in the immediate membrane vicinity measured by microelectrodes. *Biophys. J.*, **72,** 1711-1718.